Uranyl-Glycine-Water Complexes in Solution: Comprehensive Computational Modeling of Coordination Geometries, Stabilization Energies, and Luminescence Properties

ARTICLE *in* INORGANIC CHEMISTRY · FEBRUARY 2011

Impact Factor: 4.76 · DOI: 10.1021/ic200204p · Source: PubMed

4 AUTHORS, INCLUDING:

Jing Su
Shanghai Institute of Applied Physics
32 PUBLICATIONS **239** CITATIONS
SEE PROFILE

W H Eugen Schwarz
Universität Siegen
199 PUBLICATIONS **3,852** CITATIONS
SEE PROFILE

Jun Li
Tsinghua University
283 PUBLICATIONS **8,889** CITATIONS
SEE PROFILE

Inorganic Chemistry

ARTICLE

pubs.acs.org/IC

Uranyl-Glycine-Water Complexes in Solution: Comprehensive Computational Modeling of Coordination Geometries, Stabilization Energies, and Luminescence Properties

Jing Su, Kai Zhang, W. H. Eugen Schwarz,† and Jun Li*

Department of Chemistry and Laboratory of Organic Optoelectronics and Molecular Engineering of the Ministry of Education, Tsinghua University, Beijing 100084, China

Supporting Information

ABSTRACT: Comprehensive computational modeling of coordination structures, thermodynamic stabilities, and luminescence spectra of uranyl-glycine-water complexes $[UO_2(Gly)_n aq_m]^{2+}$ (Gly = glycine, aq = H_2O, $n = 0-2$, $m = 0-5$) in aqueous solution has been carried out using relativistic density functional approaches. The solvent is approximated by a dielectric continuum model and additional explicit water molecules. Detailed pictures are obtained by synergic combination of experimental and theoretical data. The optimal equatorial coordination numbers of uranyl are determined to be five. The energies of several complex conformations are competitively close to each other. In non-basic solution the most probable complex forms are those with two water ligands replaced by the bidentate carboxyl groups of zwitterionic glycine. The N,O-chelation in non-basic solution is neither entropically nor enthalpically favored. The symmetric and antisymmetric stretch vibrations of the nearly linear O−U−O unit determine the luminescence features. The shapes of the vibrationally resolved experimental solution spectra are reproduced theoretically with an empirically fitted overall linewidth parameter. The calculated luminescence origins correspond to thermally populated, near-degenerate groups of the lowest electronically excited states of $^3\Delta_g$ and $^3\Phi_g$ character, originating from $(U-O)\sigma_u \rightarrow (U\text{-}5f)\delta_u\phi_u$ configurations of the linear $[OUO]^{2+}$ unit. The intensity distributions of the vibrational progressions are consistent with U−O bond-length changes around $5^1/_2$ pm. The unusually high intensity of the short wavelength foot is explained by near-degeneracy of vibrationally *and* electronically excited states, and by intensity enhancement through the asymmetric O−U−O stretch mode. The combination of contemporary computational chemistry *and* experimental techniques leads to a detailed understanding of structures, thermodynamics, and luminescence of actinide compounds, including those with bioligands.

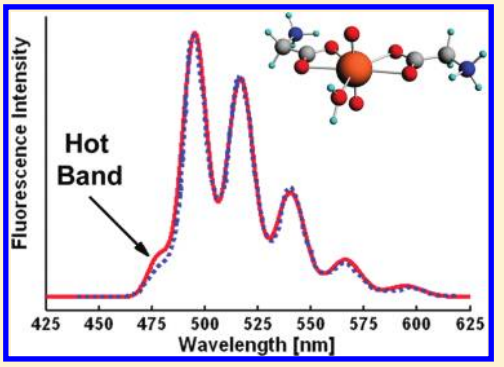

1. INTRODUCTION

Actinides exist in natural resources and man-made radioactive wastes from mineral processing, nuclear power plants, and weapons production. There are many open questions in actinide chemistry, especially concerning complexation in chemically complicated environments such as polar solvents with various coordinating ligands. The exploration of uranyl ions in the natural inventory, as a prominent example, forms the basis for active manipulation of chemical change and migration of uranium in soil, water, and food chains. It is essential to understand, at the molecular level, the interactions of the actinides with various organic ligands, for example, amino acids.[1,2]Computational chemistry is playing an important role in research on uranyl chemistry,[3] though still less so for complexation with bioligands.[4]

The coordination *structures* of actinide complexes and their *stabilities* in solution are essential data. *Luminescence* spectroscopy of uranyl compounds is particularly useful, because of its high spectral sensitivity and relatively low concentration requirement. Numerous spectroscopic data of actinide compounds have been accumulated in the literature, in particular for uranyl complexes.[5−9] Theoretical investigations have concentrated on inorganic species.[3a−3h,3j−3p,10] It is hence desirable to develop the application of available computational approaches to the geometries, stabilities, and spectra of the more complicated bio-organic uranyl complexes, in particular in solution, to underpin the relations between the electronic parameters and the measurable data.

Because of the complexity of electron correlation and relativistic effects, there exist so far no theoretical simulations of the luminescence of actinide biocomplexes. A step in this direction is the present computational modeling of uranyl-glycine-water complexes in aqueous solution. We at first briefly review the current understanding of uranyl complexes in their ground and low-lying electronically excited states, using the orbital scheme in Figure 1. Section 2 describes the state-of-the-art quantum-chemical methods applied here. Geometries and stabilities of various $[UO_2(Gly)_n aq_m]^{2+}$ complexes ($n = 0$ to 2; $m = 0$ to 5) in vacuum and aqueous environment are discussed in Section 3, adding structural details to the experimental knowledge. Section 4 is devoted to the solution spectra, based on the derived structures and

Received: March 28, 2010

   dx.doi.org/10.1021/ic200204p | *Inorg. Chem.* XXXX, XXX, 000–000

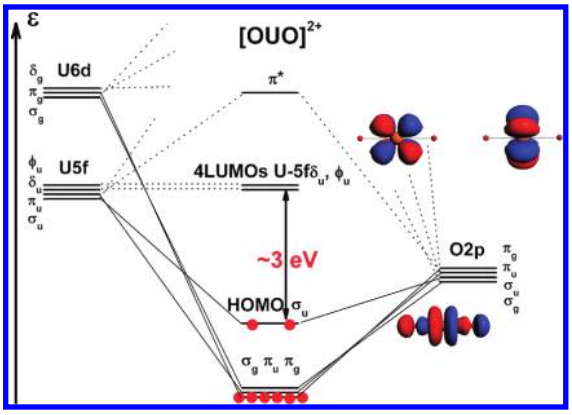

Figure 1. Valence-orbital energy levels of $[OUO]^{2+}$ and of its constitutive atoms. The vertical double-arrow indicates the electronic transitions between the U(5f)-O(2p) bonding σ_u HOMO and the nonbonding U-5f δ_u and ϕ_u LUMOs, see their orbital envelopes.

stabilities. We elucidate some problems concerning the lower electronic excitations, the excitation-induced U−O bond-length increases and the high intensities of the hot bands. Our conclusions concerning both the properties of the complexes and some methodological problems are presented in Section 5.

1.1. Uranyl-Gycine-Water Complexes. As a rather stable building block of U(VI) compounds, linear uranyl $[OUO]^{2+}$ tends to coordinate ligands in the equatorial plane. Equatorial coordination numbers CN^{eq} typically lie between 4 and 6, depending on the size and the binding strengths of the ligands. Oxygen-containing ligands preferentially coordinate with their oxygen atoms to the uranyl cation, that is, U(VI) is highly "oxophilic". The uranyl speciation in solution is difficult to characterize because of the dynamic ligand-solvent coordination complexity.[3e,3k,3n,4a,4b,10d,10e] Common bioligands comprise carboxylates, phosphates, amino-acids, peptides, proteins, and DNA. Here, we use computational chemistry to elucidate the geometric structures and thermodynamic stabilities of simple uranyl amino-acid complexes in aqueous solution. With the theoretically established geometries and solvent effects, the luminescence properties can then be predicted and exploited.

Glycine ($NH_2CH_2CO_2H$ = $^0Gly^0$) is the simplest amino acid and very common in the biosphere. It usually exists in zwitterionic form ($^+NH_3CH_2CO_2^-$ = $^+Gly^-$). Several experimental investigations of uranyl-glycine solutions were reported during the past half century.[11−15] Therefore, we start our theoretical investigations with uranyl-glycine-water complexes, where we can compare with experimental deductions, and benefit from the theory-experiment combination.

X-ray structural studies of solid uranyl-glycine complexes show that the carboxylate rather than the amino group binds to oxophilic uranium. Here, glycine does rarely act as a *chelating ligand* with its $\underline{CO_2}^-$ and $\underline{NH_2}^0$ ends forming a 5-membered ring.[15,16] Usually, mono- or *bidentate carboxylate* coordination by the R-CO_2^- ligand is observed in the crystals, forming a four-membered ring in the latter case. All that may hold true also in (non-basic) aqueous solutions. Often, monodentate coordination of the $^+Gly^-$ form is assumed. In basic solution, chelation by $\underline{NH_2}CH_2\underline{CO_2}^-$ has also been postulated.[13] Note that in solution chemistry, the word "bidentate" usually refers to 5-ring chelation, not to 4-ring coordination by the carboxylate. Anyhow, few details of the coordination geometry in solution are unequivocally known (see, for example, ref 13d).

To qualitatively understand chemical bonding and spectra of the uranyl complexes, we refer to Figure 1, where axial symmetry is assumed for simplicity of discussion.[17] The occupied 2pσ,π valence shells of the terminal oxygen anions O^{2-} are stabilized by the U-5f,6d manifold of orbitals through dative bonding of O involving σ_g, σ_u and pairs of π_u and π_g orbitals, leading to U≡O triple bonding. In the uranyl-glycin-water complexes, the highest occupied molecular orbital (MO) is the bonding (O-2p,U-5f)σ_u orbital of the O−U−O moiety, which becomes marginally perturbed by equatorial ligands. The order of the slightly lower, near-degenerate σ_g, π_u, and π_g levels depends somewhat on the equatorial coordination.

In an ionic picture, all valence electrons are assigned to O^{2-}, and uranium obtains the oxidation state U(VI). The U-7s shell is energetically pushed up upon axial coordination, common for the outer *n*s orbitals of chemically bonded transition metal atoms,[18] and can therefore be neglected in qualitative discussions, The valence shell of U(VI) comprises the empty U-5f and U-6d levels, where 5f is split into σ_u and pairs of π_u, δ_u, and ϕ_u and 6d is split into σ_g and pairs of π_g and δ_g. In the bare uranyl dication, the U-5fδ_u, 5fϕ_u, and 6dδ_g orbitals have no symmetry-matching counterparts from the O atoms and do not participate in O−U−O bonding. They remain nonbonding, low in energy, and localized on the uranium (Figure 1). However, these low-lying virtual orbitals are available for weaker σ and π donating interactions of Lewis-base ligands in the equatorial plane.

1.2. Uranyl Luminescence. Uranyl salts exhibit characteristic optical properties in absorption and emission. The practical exploitation and the scientific study have long histories.[19−21] Time-resolved laser-induced luminescence spectroscopy can provide rich information, thus becoming an advantageous experimental technique in actinide chemistry.[22] One should therefore be able to interpret and predict those properties. We will simulate the vibration-resolved experimental luminescence spectra quantum-chemically to understand the relations between the empirical details and their electronic origin. While experimental spectroscopy can yield accurate excitation energies ($\sim \pm 1$ cm^{-1}) and sometimes also tentative assignments, theoretical calculations and simulations can yield definite assignments with approximate energies, presently limited to about ± 1000 cm^{-1} for electronic excitations and a few ± 10 cm^{-1} for vibrations.

The luminescence of uranyl complexes in the visible yellow-green region is mainly due to the lowest electronically excited states of spin-triplet character, where an electron from the highest O−U−O bonding molecular orbitals (MOs) has been raised to the nonbonding U-5f levels (Figure 1). The formal oxidation state of uranium is thereby reduced to U(V), the so-called photoreduction.[23] In nonrelativistic $D_{\infty h}$ symmetry, such electronic transitions are spin, parity, and angular-momentum dipole-forbidden. The luminescence becomes allowed through relativistic spin−orbit coupling, the broken symmetry of the coordination geometry of the solvated complex ions, and asymmetric vibrations.

The experimental absorption and luminescence spectra of uranyl compounds have been extensively studied by various groups and were excellently reviewed by Denning[24,25] and others.[26−29] The luminescence spectra are characterized by vibrational progressions, usually assigned to a common electronic origin. However, we have found several "lowest excited" near-degenerate electronic states, originating from $^3\Delta_g$ and $^3\Phi_g$ terms.

The vibrational progression in the O−U−O symmetric stretching mode of the electronic ground state is dominant in

dx.doi.org/10.1021/ic200204p |*Inorg. Chem.* XXXX, XXX, 000–000

these spectra. The intensity distributions had been interpreted since the early 1960s[30] exploiting the Huang−Rhys-factor[31] for a "single metal−oxygen bond model". Different authors have deduced different expansions ΔR of the U−O bond length in the electronically excited state, differing by up to a factor of 2.[30,32] In addition to this interpretational discrepancy, there is a real scatter of ΔR-values for different excited states and for different equatorial ligands. Quantum chemical calculations in the literature[20,33,34,35a,36] often yielded significantly smaller ΔR-values.

Another open question concerns the intensity of an emission band energetically above the first strong luminescence band, which may go down with reduced temperature. A hot band from the first symmetric vibrational state of a nondegenerate, electronically excited state of O−U−O would have an intensity around 3% at room. However, in some cases these "hot band" intensities are much higher (e.g., up to 15% for uranyl glycine solutions). Knowledge of the highly resolved single crystal spectra[26−29] can be related to the broad-band solution spectra. This holds in particular for acidic aqueous uranyl solutions (as applied for the luminescence spectra to be analyzed below), since uranyl complexes maintain a low degree of hydrolysis at lower pH values (6 to 3).[37]

2. THEORETICAL METHODOLOGY AND COMPUTATIONAL DETAILS

Density functional theory (DFT) has been widely used to optimize molecular structures and energies of actinide compounds. In the Kohn-Sham formalism the Fermi and Coulomb electron correlations are approximated by a density functional (DF) in a self-consistent-field (SCF) manner. While scalar relativistic (SR) approximations seem sufficient for closed-shell ground state species, relativistic spin-orbit (SO) coupling effects must be taken into account for the structures, energies, vibrations, and optical properties involving electronically excited states. Time-dependent density functional theory (TDDFT) with SO coupling effects is nowadays being routinely applied for the vibronic actinide spectra involving low-lying electronic states, because of its reasonable accuracy at low computational cost.[35a,38]

The ground and various excited states of the naked $[UO_2]^{2+}$ ion have been extensively studied by using different variants of spin-orbit electron-correlation methods, including SO-CAS-PT2 (multiconfiguration "complete active space" SCF with second-order perturbation correction), SO−CI (configuration interaction), and SO−CC (coupled cluster).[20,33,34] SO-TDDFT reproduces the experimental vertical excitation energies of $[UO_2Cl_4]^{2-}$ within a few 1000 cm^{-1} (∼ several 0.1 eV), depending on the exchange-correlation functional used.[35a] This accuracy is somewhat inferior to that of the more sophisticated ab initio electron correlation approaches based on wave function theory (WFT), which can often reach an accuracy better than 0.1 eV.[34,36,39,40] The latter methods are usually used for benchmark calculations of small actinide systems, but are of limited value in the case of actinide complexes with bulky organic ligands. The interplay of SO coupling and ligand field effects influences the structure and energetic order of the individual electronic states. While single-point ab initio calculations are still possible (see, e.g., ref 35b), the important structure optimization at those levels becomes quite time-consuming. Therefore, our calculations were mainly performed at the SO-DFT and SO-TDDFT levels, with corrections from the SO-CAS-PT2 calculations on naked uranyl and the uranyl halides.

2.1. Energies, Structures, Stabilities, and Solvation. The geometric structures of the variously hydrated $[UO_2]^{2+}$, $[UO_2(Gly)]^{2+}$, and $[UO_2(Gly)_2]^{2+}$ complexes in their electronic ground-states were optimized using DFT methods as implemented in the Amsterdam Density Functional code (ADF 2007.01).[41] The Perdew−Burke−Ernzerhof (PBE) exchange-correlation functional was employed.[42] Uncontracted Slater basis sets of triple-ζ plus one polarization (TZP) quality for the U atom, and of double-ζ plus one polarization (DZP) quality for the H, C, N, and O atoms were selected from the ADF basis library.[43] The frozen atomic core approximation was applied to $[1s^2]$ of C, N, and O, and to $[1s^2-5d^{10}]$ of U. The zero-order regular approximation (ZORA)[44] was used to account for scalar and spin−orbit relativistic effects. The basis set superposition error (BSSE) was corrected by the counter-poise (CP) recipe, see below eq 1.[45]

Since solvation effects of strongly polar and hydrogen bonding media are significant,[3c,3e,3g,3m,4d] they need to be taken into account for uranyl-glycin-water complexes in aqueous solution. We used the polarizable continuum model COSMO.[46] We adopted the 20% reduced MM3 atomic radii,[47] the default dielectric constant for solvent water, and tried various effective radii for the solvent molecules, and both the solvent accessible surface (SAS)[48] as well as the solvent-excluding surface (SES)[49] with the radius of H as 1.08 Å. The solvation model was applied to determine the potential energy hyper-surfaces (PES) of the ground and various low-lying excited triplet states.[50] Also, the effect of water molecules added in a second solvation shell was investigated.[3c−3h,3j−3p,4a,10d,10e]

In the vibrational frequency calculations, the softness of the ligand conformations together with the computational numerical noise led in a few cases to one or two small "imaginary" frequencies ($5i-45i$ cm^{-1}). Otherwise, all frequencies were real, indicating that the structures were true minima on the energy surface. The flexibility of the ligands became suppressed upon embedding the complexes in the model solvent.

The stabilization energies of the complex formation ($\Sigma_i \mathbf{A}(i) \rightarrow \mathbf{A}$) were determined (as negative values) according to eq 1,

$$\Delta E^{\mathrm{stab}} = E_{\mathrm{A}} - \sum_i E_{\mathrm{A}}(i) + \sum_i [E_{\mathrm{A}}(i) - E_{\mathrm{A}}(i)^{\mathrm{BS(A)}}] \qquad (1)$$

A refers to the whole complex and **A**(i) to its component i. The energies E (without or with inclusion of the solvation effects) refer to species with optimized structures (in vacuum or embedded in the continuum model solvent, respectively). The last sum of brackets represents the BSSE correction; superscript BS(**A**) indicates an extended basis set for component **A**(i), comprising the basis sets of all other components as in complex **A**.

Finally, we accounted for the zero-point vibrational energy (ZPE), for the standard concentration conditions including the "translational correction" in the condensed phase, and for the thermal contributions, to obtain the Gibbs free complexation energies ΔG of the various complexes in solution at room temperature (T = 298 K). The translational, vibrational, and rotational contributions to the energy and entropy terms were calculated using the partition functions of the uncoupled translating rotator-vibrator model. The moments of inertia and the harmonic vibrational frequencies were obtained from geometry optimizations and full normal-mode analyses in the gas phase. The applied thermodynamic formulas and practical calculation examples were taken from the literature.[3m,4c,51]

2.2. Excited States and Luminescence Spectra. The equilibrium geometries R_e of the electronically excited triplet states of $^3(\sigma_u \rightarrow f\delta_w\phi_u)$ character, which are the lowest ones of their symmetry, were determined by individual DF optimizations. The vertical transition energies $\Delta E(R_e)$ were obtained by TDDFT at the electronic excited state geometries. The adiabatic transition energies were then determined by adding the ground-state energy change between the ground- and excited-state geometries.[52] The statistically averaged orbital potentials (SAOP) with correct asymptotic $1/r$ behavior were employed in the TDDFT calculations.[53] The significant SO couplings in the excited states were accounted for by the relativistic two-component ZORA formalism.[44]

The *time-dependent theory of molecular spectra*, as developed by Heller et al.[54] and later updated by Petrenko and Neese[55] had been successfully applied, for instance, to various organometallic compounds.[56] This

dx.doi.org/10.1021/ic200204p |*Inorg. Chem.* XXXX, XXX, 000–000

semiclassical vibronic approach can take several electronic PES and multimode vibrations into account. For small structural changes during the optical transition from a single PES and for small vibrational anharmonicities, the common *Franck−Condon approach*[57,58] yields similar results. The latter is more transparent to explain the influence of physical parameter changes on the spectral shape. Therefore, we also applied the Franck−Condon formulas of Struck and Fonger[57] to elucidate the luminescence band shapes of the hydrated uranyl-glycine systems (see Figure 8 below).

In this paper, we designate the transitions from electronic state i to the ground state by $(i0)$, in parentheses. The dominant luminescence transition is (10). The concomitant change of the vibrational state from v to w (of the symmetric stretching mode of the O−U−O unit, if not specified otherwise) is indicated by subscript $_{vw}$. The main band-progression is $(10)_{0w}$. Thermal excitations of the $(1)_0$ state at room temperature of the vibrational mode and of several adjacent electronic states, namely, the $(1)_1$ and $(i)_0$ states, also contribute to the luminescence. Both types will here be called hot bands, independent of vibrational or electronic excitation. The intensity of the emitted photons, as measured by photomultipliers or photodiodes, is designated by $I(\omega)$, where the angular frequency ω of the photons is just the photon energy $E = \hbar\omega$ in quantum-chemical atomic units, with $\hbar = 1$ au. Electric dipole transitions were considered in the theoretical spectra, which were eventually compared to the measured ones.[11]

3. STRUCTURE AND STABILITY OF THE COMPLEXES

Detailed values are collected in the Supporting Information, in particular also data and figures for many less stable structures not shown here explicitly.

3.1. Free and Aquo-Coordinated Uranyl. Concerning free $[UO_2]^{2+}$, the DFT results are $R_{UO} = 1.721$ Å for the U−O bond lengths, and $\omega_s = 1006/\omega_{as} = 1116$ cm^{-1} for the symmetric/antisymmetric stretching frequencies. This agrees well with a four-component CCSD(T) ab initio approach: $R_{UO} = 1.715$ Å and $\omega_s = 974$ cm^{-1}.[59] Depending on the methods and basis sets, other ab initio values scatter for R_{UO} from 1.67 to 1.75 Å and for ω_s from 968 to 1103 cm^{-1}.[20,33,34,60,61] This illustrates the accuracy of the numbers obtainable from present-day ab initio techniques.

Concerning the aquo complexes, the energetically most favorable coordination (see the Supporting Information) occurs for 5 water molecules in the equatorial plane. The optimized U−OH$_2$ distances are around 2.5 Å, common for equatorial oxygen ligands.[3h,g,o,62,63] The uranyl O−U−O axial bonds in the pentaquo complex (R = 1.770 Å, ω_s = 908 cm^{-1}) show the well-known elongation and weakening upon equatorial coordination. Solvation of $[UO_2aq_5]^{2+}$, simulated by aqueous continuum solvent embedding, has little further influence on the structure.

3.2. Mono-Glycine Complexes "M-*m*". The use of "bidentate" here indicates coordination of both oxygens of the carboxylate, not the chelation of the carboxylate and amino ends of the glycine chain, as found, for example, in some related cases.[13d,14a,14b,14f,14g]

Some of the minimum-energy structures of $[UO_2(Gly)_1aq_m]^{2+}$ in vacuum (m = 0 to 5) are shown in Figure 2. The glycine is coordinated in zwitter-ionic form to the uranium atom via the carboxylate oxygen atoms. Complexes with more than two water molecules possess more than one low-energy structure. Structure **M-3** has a bidentate carboxylate, while **M-3*** has a monodentate carboxylate, which is internally hydrogen-bonded to a coordinated H$_2$O, with CN^{eq} lower by one unit. Tetra-hydrated uranyl-glycine structures (**M-4** and **M-4***) are likewise. The penta-hydrated

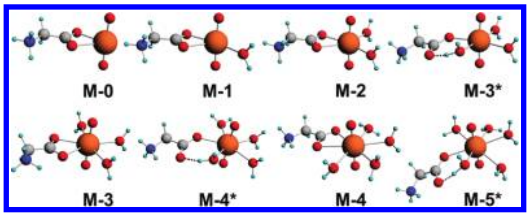

Figure 2. Complex structures of $[UO_2(Gly)aq_m]^{2+}$ in vacuum, m = 0 to 5. **M-*m*** denotes monoglycine uranyl complexes with ***m*** additional equatorial water molecules; an asterisk * indicates an internal hydrogen bond.

Table 1. Relative Complex Stabilization Energies ΔE^{stab} (in kcal/mol) of $[UO_2(Gly)aq_m]^{2+}$ in Vacuum and in the Water Model Solvent[a]

complex	structure (Figure 2)	CN^{eq}	Gly dentaticity	ΔE^{stab} (vacuum)	ΔE^{stab} (solvent)
$[UO_2(Gly)aq_2]^{2+}$	**M-2**	2	bi	-0-	-0-
$[UO_2(Gly)aq_3]^{2+}$	**M-3**	5	bi	-0-	-0-
	M-3*	4	mono	1.6	2.3
$[UO_2(Gly)aq_4]^{2+}$	**M-4***	5	mono	-0-	-0-
	M-4	6	bi	6.0	3.6
$[UO_2(Gly)aq_5]^{2+}$	**M-5***	6	mono	-0-	-0-

[a] The lowest energy structure of each $[UO_2(Gly)aq_m]^{2+}$, m = 3 to 5, defines the energy zeros -0-; without BSSE correction.

complex has only one low-lying structure **M-5***, because a bidentate glycine without an internal hydrogen bond (**M-5**) would require a crowded CN^{eq} of 7.

The uranyl U−O^{ax} distances in the monoglycine complexes are around 1.775 Å, slightly longer than in $[UO_2aq_5]^{2+}$. The carboxylate anion seems to perturb the uranyl unit a little more than two water ligands. For the various M-m complex structures the equatorial U−O^{Gly} distances vary quite a bit, between 2.32 and 2.66 Å. In the bidentate cases, the distances of U to the two O^{Gly} atoms may differ by very little or by up to 0.2 Å. This scenario is also found in the crystal structures of solid uranyl glycine complexes.[15,16]

Upon increase of CN^{eq} by 1 unit, we observe the common increase of the coordination distances, for U−O^{aq} around 0.08 Å and for U−O^{Gly} a little less. The U−O^{aq} distances of the internally hydrogen-bonded H$_2$O in the monodentate cases are about 0.08 Å shorter. Namely, hydrogen bonding makes this H$_2$O partly like a hydroxyl ion, which is known to form shorter complex bonds. Our results for glycine coordination fit into the series of literature data on uranyl coordination by various oxo-anions (CO_3^{2-}, RCO_2^-, NO_3^-).[3g,f,k,4a,4b,4d,10a,10c,10d,64]

Relative stabilization energies of some lower energy complexes in vacuum and in the model solvent are compared in Table 1. The optimal CN^{eq} = 5 is achieved by either bidentate or monodentate glycine, that is, without or with an internal hydrogen bond to an additional water ligand, respectively. In summary, several slightly different complex structures are within a few kcal/mol and might coexist in thermodynamic equilibrium, depending on the temperature, pressure, concentration, pH values, and ionic strengths.

Stabilization 'Gibbs free energies' ΔG^{stab} of the most stable structures among the **M-*m*** and **M-*m**** complexes in a dielectric solvent are compared in Figure 3. The strongly preferred CN^{eq} value is 5, with one bidentate glycine and three water molecules (M-3). Complexes with CN^{eq} = 6 are considerably higher in energy, in contrast to some crystalline uranyl compounds.[15,26b,65]

dx.doi.org/10.1021/ic200204p |*Inorg. Chem.* XXXX, XXX, 000–000

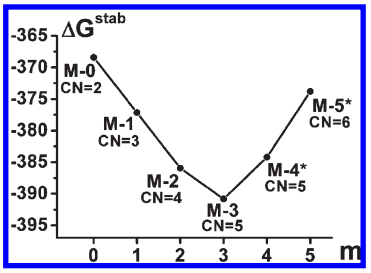

Figure 3. Stabilization Gibbs free energies ΔG^{stab} (in kcal/mol) of the most stable M-*m* structures of $[UO_2(Gly)aq_m]^{2+}$, for m = 0 to 5, see Figure 2 (optimized in vacuum, with solvation energy corrections by single-point COSMO calculations). CN denotes the equatorial coordination number. An asterisk indicates an internal hydrogen bond.

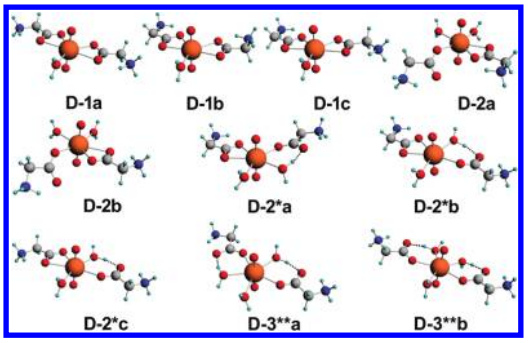

Figure 4. Structures **D-*m*** of Diglycine complexes $[UO_2(Gly)_2aq_m]^{2+}$ in vacuum for m = 1 to 3. Each asterisk indicates an internal hydrogen bond.

Our calculated results (see also the Supporting Information) indicate that CN^{eq} = 5 becomes more favored at the Gibbs free energy level, in agreement with literature results.[4d]

3.3. Di-Glycine Complexes "D-*m*". Optimized structures of $[UO_2(Gly)_2aq_m]^{2+}$ in vacuum are shown in Figure 4. Here only structures with CN^{eq} = 5 are presented because CN = 5 had already been proven to be most stable for the zero- and mono-glycine complexes, and similar trends are found for all three types of complexes. Different isomers with different directions of the amino groups are distinguished by letters a, b, c. In **D-1** type complexes $[UO_2(Gly)_2aq]^{2+}$, both glycine molecules are bidentate. In **D-2** type complexes $[UO_2(Gly)_2aq_2]^{2+}$, one glycine is bidentate and the other one is monodentate, in the **D-2*** ones with an internal hydrogen-bond. In the **D-3**** complexes, both glycines are monodentate and internally hydrogen-bonded. The two $U-O^{Gly}$ distances of the bidentate glycines are around 2.5 Å, differing by 0.06−0.12 Å. For the monodentate glycines, $U-O^{Gly}$ is near 2.35 Å (2.42 Å) in case of one (two) monodendate glycine(s) in the complex. The $U-OH_2$ distances lie between 2.45 and 2.56 Å. These trends are again consistent with experimental results of related crystal structures.[15,16,25]

The structures with low relative energies are displayed in Table 2. The energy changes due to embedding the species in the model solvent are relatively small, that is, comparable to room temperature kT (~0.6 kcal/mol). Concerning the complex species in vacuum, a water molecule in a second coordination sphere (Figure 6) yields a competitive energy, in particular if doubly hydrogen bonded (see the Supporting Information). The stabilization free energies ΔG^{stab} of the most stable conformations of the D-*m* species increase from D-1 to D-2 and to D-3 (see Figure 5).

Table 2. Relative Complex Stabilization Energies ΔE^{stab} (in kcal/mol) of $[UO_2(Gly)_2aq_m]^{2+}$ in Vacuum and in the Water Model Solvent[a]

complex	structure (Figure 4)	CN^{eq}	Gly dentaticity	ΔE^{stab} (vacuum)	ΔE^{stab} (solvent)
$[UO_2(Gly)_2aq]^{2+}$	**D-1c**	5	bi, bi	-0-	-0-
	D-1a	5	bi, bi	0.6	0.5
	D-1b	5	bi, bi	0.8	
$[UO_2(Gly)_2aq_2]^{2+}$	**D-2*b**	5	mono, bi	-0-	-0-
	D-2*c	5	mono, bi	0.5	0.4
	D-2*a	5	mono, bi	1.4	
	D-2a	5	mono, bi	6.8	
	D-2b	5	mono, bi	7.2	
$[UO_2(Gly)_2aq_3]^{2+}$	**D-3**b**	5	mono, mono	-0-	0.6
	D-3a**	5	mono, mono	0.5	-0-

[a] See footnote of Table 1.

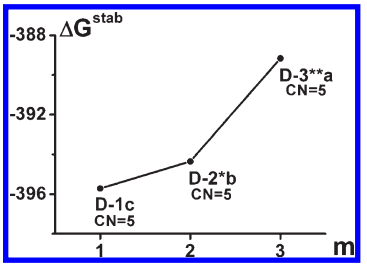

Figure 5. Stabilization free energies ΔG^{stab} (in kcal/mol) of the most stable D-*m* structures of $[UO_2(Gly)_2aq_m]^{2+}$, for m = 1 to 3, see Figure 4 (optimized in vacuum, with solvation energy corrections by single-point COSMO calculations). CN denotes the equatorial coordination number. Each asterisk indicates an internal hydrogen bond.

3.4. Uranyl-Glycine-Water Equilibria. To determine the dominant uranyl species in solution, entropy effects must be accounted for. In general, complexes with a smaller number of coordinated water molecules are favored, because H_2O has a higher entropy in the solvent than in the complex (about 35−40 $cal \cdot mol^{-1} \cdot K^{-1}$). Therefore, M-3 and D-1 species are predicted to dominate in the acidic glycine-uranyl solutions. Accounting for the zwitterionic equilibrium in water,[66]

$$^0Gly^0 \leftrightarrow {}^+Gly^- \qquad (2)$$

we have estimated the Gibbs free energies of the following two equilibria for the common standard states (55.34 mol/L for liquid water, 1 mol/L for the solutes),

$$[UO_2aq_5]^{2+} + {}^+Gly^- \rightarrow [UO_2{}^+(Gly)^-aq_3]^{2+} + 2H_2O, \quad \log_{10}(K \cdot mol/l)^{exp} \approx 1.26 \qquad (3)$$

$$[UO_2{}^+(Gly)^-aq_3]^{2+} + {}^+Gly^- \rightarrow [UO_2{}^+(Gly)^-{}_2aq_1]^{2+} + 2H_2O, \quad \log_{10}(K \cdot mol/l)^{exp} \approx 0.77 \qquad (4)$$

The relative stabilization energies of various structures with the same composition of $[UO_2(Gly)_naq_m]^{2+}$ in the solution are relatively reliable because of error cancellation. However, when comparing complexes of different composition, one has to break the hydrogen-bonds of water or zwitterionic glycine molecules in the solvent and account for less hydrogen-bonding of the coordinated species in the solvated complex. It is known that the COSMO continuum model is not accurate enough to simulate the solvation energies of species such as H_2O, $^0Gly^0$,

dx.doi.org/10.1021/ic200204p |*Inorg. Chem.* XXXX, XXX, 000–000

Table 3. Calculated Thermodynamic Quantities of Uranyl Complexation Reactions 3 and 4 [a]

complex	ΔH	ΔG	$\Delta G^{\varnothing}$	log [K]
M-4*	−11.44	−11.23	−8.84	6.5
M-3*	−6.27	−15.07	−8.37	6.1
M-3	−10.41	−22.18	−15.48	11.3
Expt	0.93[b]		−1.58[b], −1.71[c]	1.16[b], 1.26[c]
D-3**b	−9.67	3.14	1.23	−0.9
D-3**a	−9.27	2.97	1.06	−0.8
D-2*c	−6.29	−5.92	−3.53	2.6
D-2*b	−7.23	−6.52	−4.12	3.0
D-1c	−0.72	−12.18	−5.48	4.0
Expt	0.22[b]		−1.42[b], −1.05[c]	1.04[b], 0.77[c]

[a] Enthalpies ΔH and Gibbs free energies ΔG (in kcal/mol) at room temperature (T = 298.15 K), $\Delta G^{\varnothing}$ for standard state conditions; logarithm$_{10}$ of the equilibrium constants log [K, in mol/L]. Calculated with ADF and COSMO. Energies corrected for the BSSE in vacuum. [b] Ref 14c. [c] Ref 11; see also refs 13d and 14a,14b.

$^{+}Gly^{-}$, or the uranyl complexes, since the hydrogen-bonding between the first and the outer solvation shells requires the explicit treatment of the specific solvent effects.[67,68] To reduce the calculation errors, we used the experimental reaction enthalpy and free energy of eq 2.[66]

While the trends in Table 3 are qualitatively correct, the free energies are yet in error by 5 and 14 kcal/mol; the complexes in the solution are predicted significantly too stable. That is, the entropy of water molecules in the continuum solvent relative to those in the complex is overestimated by about 10 cal/mol/K. In addition, the simple COSMO model without semiempirical corrections for individual hydrogen bonds misses about 2 kcal/mol of the hydration energy of H_2O,[69,70], but there are no general estimates of the solvation energy errors of the other species. Preliminary cluster calculations indicate that such errors are around several kcal/mol per single species. In particular, the stabilization of the aquo-complex $[UO_2aq_5]^{2+}$ due to solvation is underestimated by about 10 kcal/mol in energy in comparison to the two glycine complexes. Literature data[3d−3f,3j,3k,10e,63] show that it would be sufficient for the aquo-complex to treat about 50 water molecules explicitly in the second coordination shell, and then embedding the cluster in a simple continuum solvent model. To model the perturbation by one or two glycine chains sticking into the "second" coordination shell of water molecules would probably require another 100 or more additional water molecules, or a more realistic continuum solvent model around the second shell (e.g., RS-COSMO).

Water molecules in the second solvation shell of the complexes preferentially orient their oxygen ends to one or two hydrogen atoms of the coordinated water molecules (Figure 6) or of the ammonium ends of $^{+}Gly^{-}$. In contrast, the oxygen sites of uranyl or of the coordinated glycines are less favored, which is consistent with ab initio molecular dynamics (AIMD) simulations of $UO_2^{2+}(H_2O)_x$ assemblies.[3j,63]

Finally, we have *not* found glycine as a neutral or deprotonated species in acidic solutions forming N,O-chelates, as suggested by Lagrange, Cefalo, et al.[14a,14b,14f] First, there is no entropic driving force for the internal isomerization of $[(H_2O)_3(UO_2)\underline{O_2}C\cdot CH_2\cdot NH_3]^{2+}$ to $[(H_2O)_3(UO_2)\underline{O}COH\cdot CH_2\cdot \underline{N}H_2]^{2+}$, because no water molecules are released into the solution. Only the

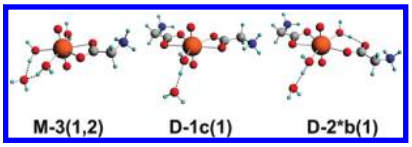

Figure 6. Representative structures (**M,D**)-*m*(***i*** **or** ***i,j***): Complexes (**M,D**)-*m* (see Figures 2 and 4) with an additional water molecule in the second solvation shell, hydrogen-bonded to coordinated H_2O molecule-(s) ***i***, or ***i*** and ***j***.

bidentate $\cdot CO_2^{-}$ is replaced by the two monodentate $\cdot COOH$ (or $\cdot COO^{-}$) and $\cdot NH_2$ end groups of a glycine. Second, there is also no enthalpic drive, at least in non-basic solution. Preliminary calculations show that N,O-chelate complexes are not favored over the bidentate carboxylate ones concerning both enthalpy and free energy in non-basic solutions where $^{+}Gly^{-}$ dominates.

4. ELECTRONICALLY EXCITED STATES AND LUMINESCENCE SPECTRA

At the beginning, we emphasize the following three points concerning the normalization of experimental and theoretical energies, transition probabilities, and band widths.

(i) *Energies* The accuracy of the DFT-calculated transition energies is at best of the order of a vibrational quantum, while the experimental accuracy is about 3 orders of magnitude better. Further improvement of the calculated energies is computationally too expensive for todays computers, so we estimated the DFT-error trends with the help of some CAS-SCF-PT2 results. In the final spectra simulations, the theoretical energy scales were shifted to get coincidence for the experimental adiabatic energies ΔE.

(ii) *Intensities* Since the experimental emission intensities are usually given in arbitrary units, we conversely fit them to the calculated ones. The height of the first strong experimental peak (at energy ΔE) is adjusted. When the lifetimes τ (1 au = 24.2 as) are solely determined by luminescence, an experimental oscillator strength f (in a.u.) can be derived from formula 5, where c_n is the velocity of light in the medium (c_n = 137.036a.u./n, refractive index of water n = 1.33).[58] However, it turns out that less than a percent of the excited states decay via optical emission.[9h−o]

$$f = c_n^{3}/\Delta E^{2}\tau \qquad (5)$$

(iii) *Band Widths* We have surveyed the fully optimized electronic wave functions, geometries, and PES along the O−U−O symmetric stretching normal mode for the ground and various electronically excited triplet states. In addition, the antisymmetric stretching, bending, and rocking modes of uranyl are also investigated for the frozen ligand system. Thereby, we get the overall intensity pattern. No effort is made to investigate the dynamics of the ligand vibrations and ligand exchange reactions, and to estimate the homogeneous and heterogeneous line broadening effects, because of the prohibitive computational expense.[3c−h,j−o,p,4a,10d,10e] Therefore, we have empirically fitted a single Gaussian width parameter Γ to all vibrational bands for each of the zero-, mono-, and diglycine complexes, as is the cases in most other computational simulation of fluorescence spectra.

dx.doi.org/10.1021/ic200204p |*Inorg. Chem.* XXXX, XXX, 000–000

Table 4. Properties of the Two Lowest-Energy SO-Coupled Groups of Electronically Excited States of $^3(\sigma_u \rightarrow f\delta_u,\phi_u)$ Triplet Character, Calculated with SO-SAOP-TDDFT

complex	DT[a]	#1[b]	$\bar{E}$[c]	ΔR_{U-O}[d]	Σf[e]	$\partial\Sigma f/\partial R$[f]	#2[b]	$\bar{E}$[c]	Σf[e]	#2/#1[g]
$[UO_2(H_2O)_5]^{2+}$	$^3\Phi_g$	2	20524	5.5	1.5	0.01	4	+762	0.6	0.03
$[UO_2(H_2O)_5]^{2+}$	$^3\Delta_g$	2	21622	4.4	0.7	−0.01	4	+777	0.5	0.10
$[UO_2(Gly)_1(H_2O)_3]^{2+}$ M-3	$^3\Delta_g$	2	21721	4.4	0.4	0.11	4	+657	4.7	0.14
$[UO_2(Gly)_2(H_2O)_1]^{2+}$ D-1c	$^3\Delta_g$	2	21830	4.5	3.1	0.09	4	+568	5.1	0.14

[a] DT = dominant $^S\Lambda_g$ ($\sigma_u^1\,\delta_u^1$ or $\sigma_u^1\,\phi_u^1$) term. [b] Number of states in the 1st (#1) and 2nd (#2) group of electronically excited states. [c] Boltzmann- and oscillator-strength weighted averages of vertical luminescence energies from the 1st group of excited states, and energy gap to the 2nd group, in cm^{-1}. [d] Change of U−O bond length upon electronic excitation, in pm. [e] Sum of Boltzmann-weighted oscillator strengths of 1st and 2nd groups of states, in 10^{-5} atomic units. [f] Asymmetric vibrational enhancement of Σf, in 10^{-5}a.u./pm. [g] Ratio of thermal populations at room temperature of 2nd to 1st group of states

Table 5. Calculated (DFT) Spectral Parameters of $[UO_2(Gly)_n(H_2O)_m]^{2+}$

complex	DT-LES[a]	ω_0[b]	ω_i[b]	ΔR_{U-O}[c]	$\Delta E(i0)$[d]	$E(i0)_{00}$[e]	$E(i0)_{adi}$[f]
$[UO_2(H_2O)_5]^{2+}$	$^3\Phi_g$	911	805	5.46	20508	21786	22347
$[UO_2(H_2O)_5]^{2+}$	$^3\Delta_g$	911	805	4.44	21613	22447	22359
$[UO_2(Gly)_1(H_2O)_3]^{2+}$**M-3**	$^3\Delta_g$	905	790	4.39	21716	22713	23083
$[UO_2(Gly)_2(H_2O)_1]^{2+}$**D-1c**	$^3\Delta_g$	902	786	4.49	21819	22911	23006

[a] Dominant $^S\Lambda$ Term (DT) of the Lowest Excited States (LES), with appreciable oscillator strength. [b] OUO symmetric stretch frequencies ω_0 and ω_i of ground (0) and excited (i) states, in cm^{-1}. [c] U−O bond length expansion ΔR_{U-O} upon electronic excitation, in pm = 0.01 Å. [d] Vertical luminescence transition energies $\Delta E(i0)$ from excited state i, in cm^{-1}. [e] OUO vibrational 0−0 transition for frozen ligand geometry, in cm^{-1}. [f] Difference between the PES minima for fully optimized complex structures, in cm^{-1}.

In the following, we discuss five features of the luminescence spectra of the zero-, mono-, and diglycine complexes: (i) the lower electronic excitation energies and the character of the wave function, (ii) the vibrational quanta of the ground and excited states, (iii) the intensity distributions of the main vibrational progression, (iv) the U−O bond length expansions of the excited states, and (v) the shorter wavelength band. The calculated data are listed in Tables 4 and 5.

(i). Groups of Low-Lying Electronic Excited States and the U-fδ/ϕ Mixing. The U-5fδ ($m_l = \pm 2$) orbitals of the OUO unit are more oriented toward the axial oxygen ligands than the U-5fϕ ($m_l = \pm 3$) ones (Figure 1). In the bare uranyl $[UO_2]^{2+}$ cation, U-5fδ is thus a little higher in energy because of the Pauli repulsion. Furthermore, the SO splitting is larger for the $m_l = \pm 3$ than for the $m_l = \pm 2$ states of U-5f type. As a result, $^3\Phi_g(\sigma_u \rightarrow 5f\phi_u)$ dominates the lowest excited energy levels of bare uranyl.[33b,34,35a]

The stronger the dative interaction in the *coordinated* uranyl complexes, the more do the equatorial ligands destabilize the U-5fϕ orbitals relative to the U-5fδ ones. This causes a reduction of the $^3\Phi_g(\sigma_u \rightarrow 5f\phi_u)$ admixture, and an increase of the $^3\Delta_g(\sigma_u \rightarrow 5f\delta_u)$ admixture in the lowest excited states of the complexes. Indeed, our TDDFT calculations predict the decreasing $^3\Phi_g$ character in the lowest states from $[UO_2(H_2O)_5]^{2+}$ to $[UO_2(Gly)_1(H_2O)_3]^{2+}$ to $[UO_2(Gly)_2(H_2O)_1]^{2+}$, and for the latter two, the $^3\Phi_g$ character is a little preferred. Previous research[35a] had shown that the TDDFT approach tends to overestimate the $^3\Phi_g$ admixture in the lowest states. Therefore, we suppose that the excited aquo-complex has more $^3\Phi_g$ admixture than the excited glycine-aquo-complexes, and that the excited glycine-aquo-complexes are already $^3\Delta_g$ dominated. Within the reliability of the method, the excitation energies are similar.

The whole low-energy triplet manifold consists of $3 \cdot (2 + 2) = 12$ individual SO states. We find the six lowest of them within about 1000 cm^{-1}, the next states are then higher by more than 2000 cm^{-1}. The lowest states cluster in two groups, see Table 4 (for more details see Supporting Information, Table S8). The two lowest ones of $^3\Delta_g$ character differ by only 20−25 cm^{-1} for $[UO_2(H_2O)_5]^{2+}$ and $[UO_2(Gly)_1(H_2O)_3]^{2+}$, and by less than 160 cm^{-1} for $[UO_2(Gly)_2(H_2O)_1]^{2+}$. The center of gravity of the second group of 4 states is 670 ± 100 cm^{-1} higher, which accidentally resembles the OUO vibrational quanta.

(ii). Symmetric Uranyl Vibration. The complexes have some 50 to 70 vibrational modes, among which about half of them lie at low frequencies and are all thermally activated. The observed first band at $E(10)_{00}$ corresponds to the 0−0 vibrational transition of O−U−O; all the other modes with slightly modified equilibrium coordinates in the excited and ground states determine the line width. That is, the experimental $E(10)_{00}$ value is adiabatic with respect to the symmetric O−U−O vibration, but vertical otherwise. The fully adiabatic luminescence energy $E(i0)_{adi}$ is also given in Table 5. The energies are determined using PBE-DFT for the ground state and SAOP-TDDFT for the excited states, with solvation and SO coupling effects included. The vibrational frequencies of the three complexes are the same within the reliability of the method, namely, ∼790 cm^{-1} for the lowest excited states, and ∼900 cm^{-1} (14% larger) for the ground states. The calculated frequency difference is ∼110 cm^{-1}, close to the experimental value at ∼130 cm^{-1}.

(iii). Overall Intensity Distribution. The luminescence spectra of uranyl compounds in solution at room temperature in the λ range of 650 to 450 nm (wavenumbers 15 to 22 × 10^3 cm^{-1}) typically consist of a dominating vibrational progression in the symmetric stretching mode of the electronic ground state of the $[O-U-O]^{2+}$ unit.[21,71] Often a low-intensity band is also detected at slightly higher energy. For instance, in the case of $[UO_2]^{2+}$ in aqueous perchloric acid, the principal part originates at 20 502 cm^{-1} with an average spacing of 855 cm^{-1}; a "hot band" appears at 768 cm^{-1} higher with less than 3% intensity ($\sim e^{-\Delta E/kT}$).[72] The experimental solution spectra of the uranyl-aquo-glycine complexes are similar, see the blue curves in Figure 7.[11]

dx.doi.org/10.1021/ic200204p |*Inorg. Chem.* XXXX, XXX, 000–000

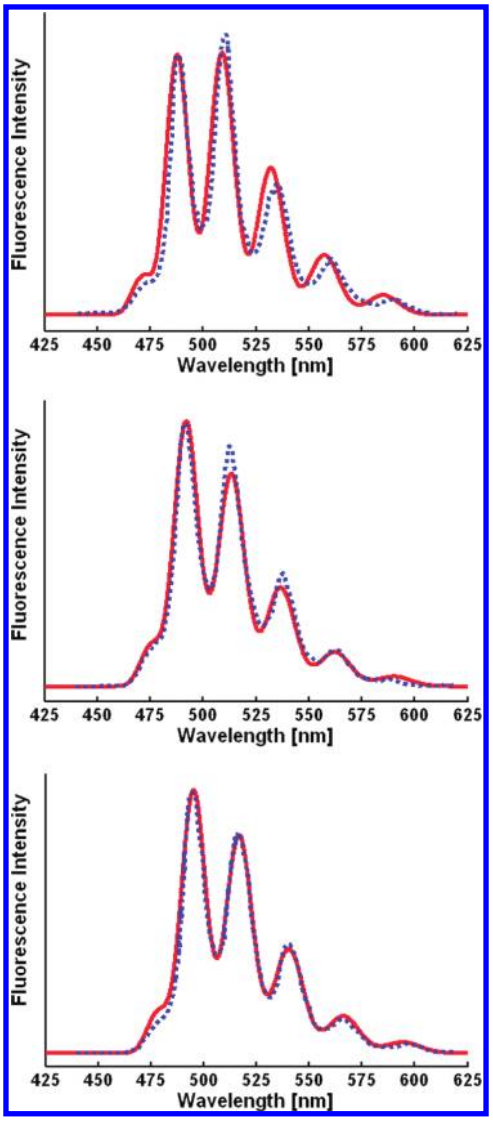

Figure 7. Luminescence spectra of $[UO_2\ aq_5]^{2+}$ (top), $[UO_2(Gly)_1\ aq_3]^{2+}$ (middle), and $[UO_2(Gly)_2aq_1]^{2+}$ (bottom). Blue, dotted lines: Experimental (obtained from Figure 4 in ref 11). Red, solid lines: theoretical.

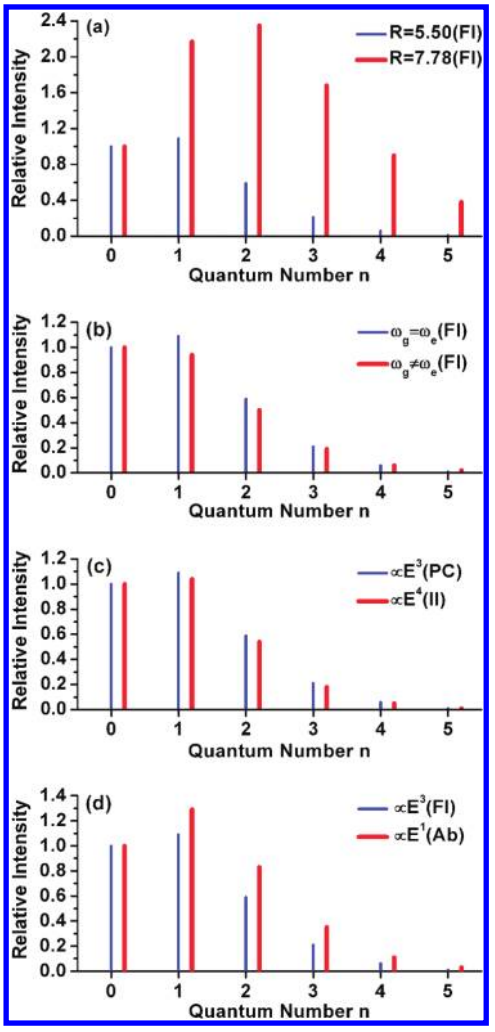

Figure 8. Intensity distributions of vibrational fluorescence (Fl) bands. (a) For a smaller and a larger ($\times\sqrt{2}$) electronically induced bond length change R. (b) For identical and different (+14%) vibrational frequencies of the initial excited (ω_e) and final ground states (ω_g). (c) For photon counting (PC) and for energy integration (II). (d) Intensity distribution of absorption (Ab) and of emission (Fl). For details see the Supporting Information.

The total intensity depends on the quantum yield, that is, the ratio of photo emission to nonradiative quenching transitions. It is known from experiments that more than 99% of the excited molecules decay radiationless, and that is hardly predictable with sufficient accuracy. However, we can determine the electronic oscillator strength $f(i0)$ at frozen geometry, and also the change due to asymmetric vibrational distortions ΔR_j of the complex structure, $\partial f(i0)/\partial \Delta R_j$. The SO coupling and static symmetry breaking in the complex induce electric dipole transition moments with oscillator strength of the order of 10^{-5} a.u. for the case of clamped nuclei. Together with asymmetric vibrational amplitudes of several pm and $\partial \Sigma f/\partial R$ values of a few 10^{-6} a.u./pm, similar transition probabilities are obtained for all three complexes, and larger ones for the second than for the first group of states.

For the two glycine complexes, the most intense band is the first 0−0 one, the intensities of the lower energy bands decreasing steadily. For the pure aquo-complex, however, the second 0−1 band is strongest, and the intensity decrease is less pronounced. This difference is due to different U−O bond length changes upon electronic excitation.

(iv). U−O Bond Expansions upon Electronic Excitations. The physically most relevant parameter of the spectral intensity distribution of a vibrational progression is the Huang−Rhys factor S[31] for the initial and final vibrational normal modes of the respective electronic states. S is approximately related to the intensity ratio of the first two bands, $I_1/I_0 \approx S$, and to the index w of the strongest band, $I_{max} \approx I_{w\approx S}$. S connects the spectral shape to the bond length change ΔR upon the electronic transition. In the case of absence of anharmonicities, Dushinsky rotations, and vibrational frequency changes, the relation simplifies to eq 6, with $z = 1$.

$$\mu \cdot \omega \cdot \Delta R_{OO}{}^2 = 2z \cdot S \qquad (6)$$

Here μ is the effective vibrating mass (for the symmetric stretch of O−U−O, μ is $M(O)/2$), ΔR_{OO} is the change of the O−O distance ($\Delta R_{OO} = 2 \cdot \Delta R_{U-O}$), and $\omega = \sqrt{k/\mu}$ is the vibrational

dx.doi.org/10.1021/ic200204p |Inorg. Chem. XXXX, XXX, 000–000

quantum ($k = k_{UO}/2$, all in a.u.). However, applying the above-mentioned "single metal−oxygen bond model" to O−U−O corresponds to $z = 2$, while the deduction of Wong et al.[32] seems to correspond to $z = 4$. For uranyl, this means $\Delta R(U-O) \approx \sqrt{S}$ **0.05** Å (our theoretical result) with $z = 1$, $\approx \sqrt{S}$ **0.07** Å (the common experimental deduction) with $z = 2$, or $\approx \sqrt{S}$ **0.11** Å (Wong's result) with $z = 4$.

Figure 8 displays the dependence of the intensity distributions of the vibrational fluorescence progression.[57,58,73] An increase of the bond-length expansion upon electronic excitation from 5.5 to 7.78 pm, that is, by a factor of $\sqrt{2} \approx 0.07/0.05$, changes the spectral shape completely (Figure 8a). The effect of change of the vibrational frequencies from initial to final electronic state (here by +14%) is smaller, though not negligible (Figure 8b). There is a quite small change of the spectral curves, when either photons are counted or the energy flux is integrated, to measure the intensities (Figure 8c). The spectral shapes for absorption and emission between the same states are also remarkably different (Figure 8d).

Table 6. U−O Bond Length Expansion ΔR (in pm = 0.01 Å) of Uranyl Compounds upon Electronic Excitations ($U^{\delta+}O^{\delta-}$) $\sigma_u \rightarrow$ (U-5f)δ_u (in Parentheses: ($U^{\delta+}O^{\delta-}$)$\sigma_u \rightarrow$ (U-5f)ϕ_u) by Using Different Theoretical and Experimental Approaches

	theoretical method[a]							
	DFT		MC-PT		CC		CI	ref.[b]
molecule	SR	SO	SR	SO	SR	SO	SO	
$[UO_2]^{2+}$		6.0 (7.2)	5.7 (7.7)	5.7 (7.4)			6.5 (7.1)	34,35a 20
	4.8 (6.8)		5.0 (6.8)		4.8 (6.3)	5.3 (6.4)		33b
						4.1 (3.6)		33a
			5.5 (7.2)	5.5 (7.0)				thw
$[UO_2F_2]$	4.4 (5.5)		4.8 (6.6)	5.2 (6.0)	5.8 (7.5)	6.2 (7.0)		thw
$[UO_2Cl_2]$	2.8 (3.7)		4.2 (5.8)	4.6 (5.3)	4.8 (6.2)	5.4 (5.9)		thw
$[UO_2Cl_4]^{2-}$		3.7 (3.9)	5.3 (7.2)	5.3 (6.3)			6.2 (7.8)	34,35a 36
$[UO_2(Gly)aq_3]^{2+}$	4.4							
Derived from Experimental Spectra Using the Single Bond Model								
$[UO_2Cl_4]^{2-}$			6.5 to 7.5					24
			7.0					27b

[a] CC, single reference coupled cluster; CI, configuration interaction; DFT, density functional theory; MC-PT, multiconfigurational 2nd-order perturbation theory (CASPT2); SO, spin−orbit coupled relativistic; SR, scalar relativistic. [b] thw = this work.

On this background, we have simulated the fluorescence spectra of the three complexes. Geometries, frequencies, and transition energies of small uranyl species, such as $[UO_2]^{2+}$, $[UO_2X_2]$ (X = F, Cl) or $[UO_2Cl_4]^{2-}$, have been reliably determined by more sophisticated ab initio methods.[20,33,34,36] As shown in Table 6, the bond-length expansions upon electronic (U−O)$\sigma_u \rightarrow$(U5f)$\delta_w\phi_u$ excitations are somewhat underestimated by DFT, possibly because of a large self-interaction error (SIE) of the compact U5f orbital.[39] According to this theoretical finding, we enlarge our DFT values of ΔR by 3/4 pm. In the case of the pure aquo complex, we apply the average of the $^3\Delta_g$ and $^3\Phi_g$ values.

Concerning the mean anharmonic vibrational frequencies, they are usually somewhat smaller than the harmonic ones, in particular at the DFT level of approximation. This is also the case here, as shown in Table 7, where we have reduced the harmonic OUO vibrational frequencies from DFT by an average value of 60 cm^{-1}. The electronic excitation energies from SO-TDDFT with SAOP potential also tend to be large, as compared to SO−CC or CASPT2 calculations.[33b,34,35a] We have finally shifted the calculated excitation energies to the experimental ones (displayed in Table 7) and then simulated the luminescence spectra in Figure 7 with the other calculated parameters. An optimized empirical fit of similar quality is shown in the Supporting Information.

(v). Weak High-Energy Band. Fast internal conversion (here within ps) populates the singlet ground state and a little also the SO coupled lower excited states of triplet character, which then slowly decay by luminescence (here within microseconds).[3a,11,19] The luminescence usually occurs from the lowest electronically excited state $i = 1$ to the ground state $i = 0$.[74] In the present case, however, the two lowest electronically excited states (1) and (2) are near-degenerate and contribute both to the main progression of ~700 cm^{-1}. They are designated as $(10)_{0w}+(20)_{0w}$, where w indicates the final vibrational state of the electronic ground state. The Franck−Condon factors are such that significant intensities are obtained for the first two vibrational emission bands $w = 0$ and $w = 1$, and decreasing intensities for the following ones, $w = 2, 3, 4$.

In addition, the spectra of all three complexes exhibit a high-energy foot on the left side of the first vibrational band with ~12% of its intensity (Figure 7). Within several hundred cm^{-1}, there are several energy levels that remain thermally populated,

Table 7. DFT-Theoretical (theor), ab initio Corrected (corr) and Experimentally Derived (exp deriv) Parameters for $[UO_2(Gly)_n(H_2O)_m]^{2+}$ Complexes[a]

	ω_0 [cm^{-1}]		ω_1 [cm^{-1}]		ΔR [pm]		relative hot band intensity[b]		E_{00} [cm^{-1}]	Γ [cm^{-1}]
complex	theor corr	exp deriv	theor corr	exp deriv	theor corr	exp deriv	theor	exp deriv	exp deriv	exp deriv
$[UO_2(H_2O)_5]^{2+}$	851	866	745	739	5.70	5.94	0.148	0.115	20496	221
$[UO_2(Gly)_1(H_2O)_3]^{2+}$ M-3	845	847	730	710	5.14	5.56	0.155	0.134	20321	235
$[UO_2(Gly)_2(H_2O)_1]^{2+}$ D-1c	842	830	726	710	5.24	5.33	0.157	0.111	20190	235

[a] The theoretical spectra simulation in Figure 7 is based on the theoretical, corrected values for ω_0, ω_1, and ΔR, the theoretical hot band intensity, and the experimentally derived adiabatic energy E_{00} and bandwidth Γ. [b] In comparison to the first main band, both having contributions from the first two, and the next four electronically excited states, and from the vibrationally excited states.

dx.doi.org/10.1021/ic200204p |Inorg. Chem. XXXX, XXX, 000–000

each by a few % according to the Boltzmann factor at room temperature (e.g., by 3% for 700 cm^{-1}). They can contribute to the optical emission as well. First, there is the first excited state of the symmetric OUO *vibration* that will give rise to a common "hot band" of about 2−3% intensity. An irregular progression overlays the main progression, but cannot be discriminated experimentally. In addition, there are another 4 *electronic* states (3) to (6) in the same energy region as the first OUO vibration of the lowest two excited states, that is, around 700 cm^{-1}. Their first bands $(i0)_{00}$, i = 3−6, contribute 10 to 14% to the high-energy foot. Therefore, the foot is about 4 to 5 times stronger than a common hot band. Finally, we note that the oscillator strengths of the lower excited states are also modified by asymmetric vibrations ($\partial\Sigma f/\partial R$). Therefore, the vibrational excitation of the antisymmetric O−U−O stretching mode may also contribute to the high-energy foot.

5. CONCLUSIONS

The computational simulations of complexation, solvation, and optical behavior of the actinides are topical challenges. The results of this work show that competing complex geometries, relative stabilities, and luminescence properties of uranyl-glycin-water solutions can be reproduced by relativistic DFT approaches, provided they are partially corrected on the basis of ab initio model calculations and with the help of some experimental data. The application of realistic solvent models is imperative. The experimental trends can be explained, and additional details can be specified through theory.

Relativistic scalar and spin−orbit coupling effects, but in particular the complicated electron-correlation effects in the partially diffuse, partially compact valence shells of the actinide compounds, must be treated very carefully. Present density functional approximations still require significant calibration by more reliable post-SCF results of model molecules. Simple continuum solvent models need corrections from explicitly calculated interactions to the second coordination sphere or by some empirical adjustment. Present computational modeling of actinide solution chemistry cannot compete with the spectroscopic accuracy of experimental band energies; nor can absolute luminescence intensities be obtained ab initio in routine investigations because of the complexity of various nonradiative processes. However, the relative energies and intensity distributions of the luminescence spectra can be predicted.

In solution, the uranyl-glycine-water complexes have various conformations and isomers, even complexes with different sum formulas may have similar stabilities. We have shown that at room temperature, five-coordination in the equatorial plane of uranyl is favored in aqueous solution because of enthalpic and entropic reasons. In neutral to acidic solutions, one or two glycine molecules bind as zwitterions with their bidentate carboxylic groups, with water molecules occupying the remaining space in the first coordination sphere. Further structural details of the first and second coordination sphere have been added to the experimentally derived knowledge. Different orientations of the glycine chains exist in equilibrium. The water molecules in the second solvation shell prefer hydrogen bonding with their oxygen ends to the water and ammonium protons, instead of bonding with their hydrogen ends to the oxygen ions of uranyl or glycine. At low temperature and in the gas phase, uranyl-glycine complexes may bind more water molecules, for instance, with internal hydrogen bonding to monodentate glycine.

We find that the vibration of the whole O−U−O group rather than of a single U−O bond needs to be considered, when analyzing the vibrational progression of the symmetric O−U−O stretching mode. The U−O bond length expansion ΔR upon electronic excitation from $(U-O)\sigma_u$ to $(U\text{-}5f)\phi_u\delta_u$ is around 5.5 pm, that is, smaller than 7 pm. The lowest electronic excited states of $\sigma_u \rightarrow f\phi_u\delta_u$ type change their character from more ϕ_u and less δ_u ($\Delta_g(1^3\Phi_g)$ derived states) for gas-phase uranyl to more δ_u and less ϕ_u ($\Pi_g(1^3\Delta_g)$ derived states) for the mono- and diglycine complexes. The pure aquo-complex is intermediate. This explains the larger ΔR of the uranyl-aquo complex in comparison to the uranyl-glycine complexes. The unusually high intensity of the high-energy foot of the progression is explained by an overlay of vibrational hot bands and emission from thermally populated, electronically excited states accidentally near-degenerate with the first O−U−O vibrationally excited state. The asymmetric O−U−O vibration contributes to all bands.

Our present approach of modeling the solvation structures and luminescent properties of uranyl-glycine-water complexes can be extended to other actinyl complexes in general. Such research will help a better understanding of the interaction of actinyl units with various common ligands, including those of geologic and biologic interest. While the computational modeling can offer additional details and insights, some thermodynamic and spectroscopic trends can only be predicted by more sophisticated theoretical approaches which are extremely computationally expensive even with today's supercomputers. More accurate theoretical approaches with more reliable electron correlation and more realistic solvation models are needed for the presently unexplained thermodynamic and spectroscopic properties.

■ ASSOCIATED CONTENT

Supporting Information. Cartesian coordinates, total binding energies of all complexes, vertical excited energies, and fluorescence intensity distributions used in Figure 8. This material is available free of charge via the Internet at http://pubs.acs.org.

■ AUTHOR INFORMATION

Corresponding Author

*E-mail: junli@tsinghua.edu.cn.

Present Addresses

†Also at Theoretical Chemistry, University of Siegen, 57068 Siegen, Germany; E-mail: schwarz@chemie.uni-siegen.de.

■ ACKNOWLEDGMENT

This work was supported by NKBRSF (2011CB932400) and NSFC (20933003, 11079006, 91026003) of China. The calculations were performed by using supercomputers at the Computer Network Information Center, Chinese Academy of Sciences, the Shanghai Supercomputing Center, and Tsinghua National Laboratory for Information Science and Technology.

■ REFERENCES

(1) (a) Taylor, D. M. *J. Alloys Compd.* **1998**, *271*−*273*, 6. (b) Guilmette, R. A. *J. Alloys Compd.* **1998**, *271*−*273*, 66. (c) Stradling, G. N. *J. Alloys Compd.* **1998**, *271*−*273*, 72.(d) Wolf, S. F. In *The Chemistry of the Actinide and Transactinide Elements*,3rd ed.; Morss, L. R.,

Edelstein, N. M., Fuger, J., Katz, J. J., Eds.; Springer: Dordrecht, The Netherlands, 2006; Vol. 5, Chapter 30; (e) Durbin, P. W. In *The Chemistry of the Actinide and Transactinide Elements*, 3rd ed.; Morss, L. R., Edelstein, N. M., Fuger, J., Katz, J. J., Eds.; Springer: Dordrecht, The Netherlands, 2006; Vol. 5, Chapter 31.

(2) (a) Szigethy, G.; Xu, J.; Gorden, A. E. V.; Teat, S. J.; Shuh, D. K.; Raymond, K. N. *Eur. J. Inorg. Chem.* **2008**, 2143–2147. (b) Gorden, A. E. V.; Xu, J.; Szigethy, G.; Oliver, A.; Shuh, D. K.; Raymond, K. N. *J. Am. Chem. Soc.* **2007**, *129*, 6674. (c) Gramer, C. J.; Raymond, K. N. *Inorg. Chem.* **2004**, *43*, 6397. (d) Veeck, A. C.; White, D. J.; Whisenhunt, D. W., Jr.; Xu, J.; Gorden, A. E. V.; Romanovski, V.; Hoffman, D. C.; Raymond, K. N. *Solvent Extr. Ion Exch.* **2004**, *22*, 1037. (e) Xu, J.; Gorden, A. E. V.; Raymond, K. N. *Eur. J. Org. Chem.* **2004**, 3244. (f) Guilmette, R. A.; Hakimi, R.; Durbin, P. W.; Xu, J.; Raymond, K. N. *Radiat. Prot. Dosim.* **2003**, *105*, 527. (g) Gorden, A. E. V.; Xu, J.; Raymond, K. N.; Durbin, P. W. *Chem. Rev.* **2003**, *103*, 4207. (h) Xu, J.; Durbin, P. W.; Kullgren, B.; Ebbe, S. N.; Uhlir, L. C.; Raymond, K. N. *J. Med. Chem.* **2002**, *45*, 3963.

(3) (a) Tsushima, S.; Götz, C.; Fahmy, K. *Chem.—Eur. J.* **2010**, *16*, 8029; (b) Páez-Hernández, D.; Ramírez- Tagle, R.; Codorniu-Hernández, E.; Montero-Cabrera, L. A.; Arratia-Pérez, R. *Polyhedron* **2010**, *29*, 975; (c) Wåhlin, P.; Schimmelpfennig, B.; Wahlgren, U.; Grenthe, I.; Vallet, V. *Theor. Chem. Acc.* **2009**, *124*, 377; (d) Cao, Z.; Balasubramanian, K. *J. Chem. Phys.* **2009**, *131*, 164504; (e) Bühl, M.; Sieffert, N.; Wipff, G. *Chem. Phys. Lett.* **2009**, *467*, 287; (f) Frick, R. J.; Hofer, T. S.; Pribil, A. B.; Randolf, B. R.; Rode, B. M. *J. Phys. Chem. A* **2009**, *113*, 12496; (g) Austin, J. P.; Sundararajan, M.; Vincent, M. A.; Hillier, I. H. *Dalton Trans.* **2009**, 5902; (h) Wåhlin, P.; Danilo, C.; Vallet, V.; Réal, F.; Flament, J.-P.; Wahlgren, U. *J. Chem. Theory Comput.* **2008**, *4*, 569; (i) Sundararajan, M.; Campbell, A. J.; Hillier, I. H. *J. Phys. Chem. A* **2008**, *112*, 4451; (j) Nichols, P.; Bylaska, E. J.; Schenter, G. K.; de Jong, W. *J. Chem. Phys.* **2008**, *128*, 124507; (k) Bühl, M.; Diss, R.; Wipff, G. *Inorg. Chem.* **2007**, *46*, 5196; (l) Tsushima, S. *J. Phys. Chem. A* **2007**, *111*, 3613; (m) Gutowski, K. E.; Dixon, D. A. *J. Phys. Chem. A* **2006**, *110*, 8840; (n) Infante, I.; van Stralen, B.; Visscher, L. *J. Comput. Chem.* **2006**, *27*, 1156; (o) Shamov, G. A.; Schreckenbach, G. *J. Phys. Chem. A* **2005**, *109*, 10961; (p) **2006**, *110*, 12072. (q) Bühl, M.; Diss, R.; Wipff, G. *J. Am. Chem. Soc.* **2005**, *127*, 13506.

(4) (a) Kubicki, J. D.; Halada, G. P.; Jha, P.; Phillips, B. L. *Chem. Cent. J.* **2009**, *3*, 10. (b) Gutowski, K. E.; Cocalia, V. A.; Griffin, S. T.; Bridges, N. J.; Dixon, D. A.; Rogers, R. D. *J. Am. Chem. Soc.* **2007**, *129*, 526. (c) Kremleva, A.; Krüger, S.; Rösch, N. *Inorg. Chim. Acta* **2009**, *362*, 2542. (d) Ray, R. S.; Krüger, S.; Rösch, N. *Dalton Trans.* **2009**, 3590.

(5) (a) Wilkerson, M. P.; Berg, J. M. *J. Phys. Chem. A* **2008**, *112*, 2515. (b) Wilkerson, M. P.; Arrington, C. A.; Berg, J. M.; Scott, B. L. *J. Alloys Compd.* **2007**, *444−445*, 634. (c) Wilkerson, M. P.; Berg, J. M.; Hopkins, T. A.; Deweya, H. J. *J. Solid State Chem.* **2005**, *178*, 584. (d) Wilkerson, M. P.; Barefield, J. E.; Berg, J. M.; Dewey, H. J.; Hopkins, T. A. *J. Nucl. Sci. Technol.* **2002**, No. Suppl. 3, 129–131. (e) Saracino, G. A. A.; Improta, R.; Barone, V. *Chem. Phys. Lett.* **2003**, *373*, 411. (f) Talbot-Eeckelaers, C.; Pope, S. J. A.; Hynes, A. J.; Copping, R.; Jones, C. J.; Taylor, R. J.; Faulkner, S.; Sykes, D.; Livens, F. R.; May, I. *J. Am. Chem. Soc.* **2007**, *129*, 2442.

(6) (a) Shi, Z.; Liu, C.; Zachara, J. M.; Wang, Z.; Deng, B. *Environ. Sci. Technol.* **2009**, *43*, 8344. (b) Wang, Z.; Zachara, J. M.; Liu, C.; Gassman, P. L.; Felmy, A. R.; Clark, S. B. *Radiochim. Acta* **2008**, *96*, 591. (c) Chang, H.-S.; Korshin, G. V.; Wang, Z.; Zachara, J. M. *Environ. Sci. Technol.* **2006**, *40*, 1244. (d) Wang, Z.; Felmy, A. R.; Xia, Y.; Buck, E. C. *J. Alloys Compd.* **2006**, *418*, 166. (e) Wang, Z.; Zachara, J. M.; McKinley, J. P.; Smith, S. C. *Environ. Sci. Technol.* **2005**, *39*, 2651. (f) Wang, Z.; Zachara, J. M.; Gassman, P. L.; Liu, C.; Qafoku, O.; Yantasee, W.; Catalano, J. G. *Geochim. Cosmochim. Acta* **2005**, *69*, 1391. (g) Wang, Z.; Zachara, J. M.; Yantasee, W.; Gassman, P. L.; Liu, C.; Joly, A. G. *Environ. Sci. Technol.* **2004**, *38*, 5591.

(7) Heaven, M. C. *Phys. Chem. Chem. Phys.* **2006**, *8*, 4497.

(8) Geipel, G. *Coord. Chem. Rev.* **2006**, *250*, 844.

(9) (a) Ansoborlo, E.; Bion, L.; Doizi, D.; Moulin, C.; Lourenco, V.; Madic, C.; Cote, G.; van der Lee, J.; Moulin, V. *Radiat. Prot. Dosim.* **2007**, *127*, 97. (b) Sinkov, S. I.; Choppin, G. R.; Taylor, R. J. *J. Solution Chem.* **2007**, *36*, 815. (c) Dozol, M.; Hagemann, R. *Pure Appl. Chem.* **1993**, *65*, 1081. (d) Amayri, S.; Arnold, T.; Reich, T.; Foerstendorf, H.; Geipel, G.; Bernhard, G.; Massanek, A. *Environ. Sci. Technol.* **2004**, *38*, 6032. (e) Markich, S. *J. Sci. World J* **2002**, *2*, 707. (f) Huang, H.; Chaudhary, S.; van Horn, J. D. *Inorg. Chem.* **2005**, *44*, 813. (g) Xie, W.; Badawi, A.; Huang, H.; van Horn, J. D. *J. Inorg. Biochem.* **2009**, *103*, 58. (h) Meinrath, G.; Lis, S.; Stryla, Z.; Noubactep, C. *J. Alloys Compd.* **2000**, *300−301*, 107. (i) Christiane Görller-Walrand, C.; De Houwer, S.; Fluyt, L.; Binnemans, K. *Phys. Chem. Chem. Phys.* **2004**, *6*, 3292. (j) Billard, I. *Appl. Spectrosc.* **2003**, *57*, 1027. (k) Wang, G.; Su, Y.; Monts, D. L. *J. Phys. Chem. A* **2008**, *112*, 10502. (l) Formosinho, S. J. *Photochem. Photobiol. Sci.* **2003**, *2*, 569. (m) Billard, I.; Rustenholtz, A.; Sémon, L.; Lützenkirchen, K. *Chem. Phys.* **2001**, *270*, 345. (n) Bouby, M.; Billard, I.; Bonnenfant, A.; Klein, G. *Chem. Phys.* **1999**, *240*, 353. (o) Ke, H-Y. D.; Rayson, G. D. *Appl. Spectrosc.* **1992**, *46*, 1376.

(10) (a) de Jong, W. A.; Aprà, E.; Windus, T. L.; Nichols, J. A.; Harrison, R. J.; Gutowski, K. E.; Dixon, D. A. *J. Phys. Chem. A* **2005**, *109*, 11568. (b) García-Hernández, M.; Willnauer, C.; Krüger, S.; Moskaleva, L. V.; Rösch, N. *Inorg. Chem.* **2006**, *45*, 1356. (c) Vallet, V.; Macak, P.; Wahlgren, U.; Grenthe, I. *Theor. Chem. Acc.* **2006**, *115*, 145. (d) Schlosser, F.; Krüger, S.; Rösch, N. *Inorg. Chem.* **2006**, *45*, 1480. (e) Bühl, M.; Sieffert, N.; Golubnychiy, V.; Wipff, G. *J. Phys. Chem. A* **2008**, *112*, 2428. (f) Ruipérez, F.; Wahlgren, U. *J. Phys. Chem. A* **2010**, *114*, 3615.

(11) Günther, A.; Geipel, G.; Bernhard, G. *Polyhedron* **2007**, *26*, 59.

(12) Gharib, F.; Mojtabaei, R. *Russ. J. Inorg. Chem.* **2005**, *50*, 1536.

(13) (a) Szabó, Z.; Grenthe, I. *Inorg. Chem.* **2000**, *39*, 5036. (b) Jiang, J.; Renshaw, J. C.; Sarsfierld, M. J.; Livens, F. R.; Collison, D.; Charnock, J. M.; Eccles, H. *Inorg. Chem.* **2003**, *42*, 1233. (c) Rao, L.-F.; Garnov, A. Y.; Jiang, J.; Di Bernardo, P.; Zanonato, P. L.; Bismondo, A. *Inorg. Chem.* **2003**, *42*, 3685. (d) Moll, H.; Geipel, G.; Reich, T.; Bernhard, G.; Fanghanel, T.; Grenthe, I. *Radiochim. Acta* **2003**, *91*, 11. (e) Feldman, I.; Koval, L. *Inorg. Chem.* **1963**, *2*, 145. (f) Chaudbari, B. S.; Kelkar, S. S.; Nemade, B. I. *J. Electrochem. Soc. India* **1981**, *31*, 143.

(14) (a) Lagrange, P.; Schneider, M.; Lagrange, J. *J. Chim. Phys. Phys.-Chim. Biol.* **1998**, *95*, 2280. (b) Lagrange, P.; Schneider, M.; Zare, K.; Lagrange, J. *Polyhedron* **1994**, *13*, 861. (c) Bismondo, A.; Rizzo, L.; Tomat, G.; Curto, D.; Di Bernardo, P.; Cassol, A. *Inorg. Chim. Acta* **1983**, *74*, 21. (d) Dongre, V. G.; Dhuley, D. G. *Curr. Sci.* **1980**, *49*, 305. (e) Ramanujam, V. V.; Rengaraj, K.; Sivasankar, B. *Bull. Chem. Soc. Jpn.* **1979**, *52*, 2713. (f) Cefola, M.; Taylor, R. C.; Gentile, P. S.; Celiano, A. C. *J. Phys. Chem.* **1962**, *66*, 790. (g) Farook, O.; Malik, A. U.; Ahmad, N.; Rahman, S. M. F. *J. Electroanal. Chem.* **1970**, *24*, 464. (h) Sergeev, G. M.; Korshunov, I. A. *Radiokhimiya* **1973**, *15*, 621. (i) Singh, S.; Yadava, L.; Yadava, P. C.; Yadava, K. L. *Bull. Soc. Chim. France Part. 1* **1984**, *11−12*, 349.

(15) Alcock, N. W.; Flanders, D. J.; Kemp, T. J.; Shand, M. A. *J. Chem. Soc., Dalton Trans.* **1985**, 517.

(16) Keramidas, A. D.; Rikkou, M. P.; Drouza, C.; Raptopoulou, C. P.; Terzis, A.; Pashalidis, I. *Radiochim. Acta* **2002**, *90*, 549.

(17) See also ref 24; as the orbital energies$_i$ of a molecular system strongly depend on the system's overall charge and environment, the relative positions of the energy levels of the free atomic ions, of the free $[OUO]^{2+}$ unit, and of the complex ions in solution are shifted, which makes Figure 1 schematic.

(18) (a) Wang, S. G.; Qiu, Y. X.; Fang, H.; Schwarz, W. H. E. *Chem.—Eur. J.* **2006**, *12*, 4101. (b) Schwarz, W. H. E. *J. Chem. Educ.* **2010**, *87*, 444.

(19) Ghosh, R.; Mondal, J. A.; Ghosh, H. N.; Palit, D. K. *J. Phys. Chem. A* **2010**, *114*, 5263.

(20) Zhang, Z.; Pitzer, R. M. *J. Phys. Chem. A* **1999**, *103*, 6880.

(21) Rabinowitch, E.; Belford, R. L. *Spectroscopy and Photoechemisty of Uranyl Compounds*; Oxford University Press: Oxford, U.K., 1964.

(22) Szabó, Z.; Toraishi, T.; Vallet, V.; Grenthe, I. *Coord. Chem. Rev.* **2006**, *250*, 784.

(23) Tsushima, S. *Inorg. Chem.* **2009**, *48*, 4856.

(24) Denning, R. G. *J. Phys. Chem. A* **2007**, *111*, 4125.

(25) Denning, R. G. *Struct. Bonding (Berlin)* **1992**, *79*, 215.
(26) (a) Denning, R. G.; Snellgrove, T. R.; Woodwark, D. R. *Mol. Phys.* **1976**, *32*, 419. (b) Denning, R. G.; Foster, D. N. P.; Snellgrove, T. R.; Woodwark, D. R. *Mol. Phys.* **1979**, *37*, 1089. (c) Barker, T. J.; Denning, R. G.; Thorne, J. R. G. *Inorg. Chem.* **1973**, *26*, 1721.
(27) (a) Moran, D. M.; Metcalf, D. H.; Richardson, F. S. *Inorg. Chem.* **1992**, *31*, 819. (b) Metcalf, D. H.; Dai, S.; Del Cul, G. D.; Toth, L. M. *Inorg. Chem.* **1995**, *34*, 5573.
(28) Flint, C. D.; Tanner, P. A. *J. Chem. Soc., Faraday Trans. II* **1978**, *74*, 2210.
(29) (a) Nichols, E. L.; Howes, H. L.; Wick, F. G. *Phys. Rev.* **1919**, *14*, 201. (b) Volod'ko, L. V.; Komyak, A. I.; Vitkovskli, G. P.; Sleptsov, S. E. *J. Appl. Spectrosc.* **1974**, *20*, 480.
(30) (a) Jeżowska-Trzebiatowska, B.; Bartecki, A. *Spectrochim. Acta* **1962**, *18*, 799. (b) Ballhausen, C. J. *Theor. Chim. Acta (Berl.)* **1963**, *1*, 285.
(31) Huang, K.; Rhys, A. *Proc. R. Soc., London* **1973**, *204A*, 406.
(32) Wong, D. P.; Wong, A. Y. C.; Wong, E. Y. *J. Chem. Phys.* **1972**, *56*, 2838.
(33) (a) Réal, F.; Gomes, A. S. P.; Visscher, L.; Vallet, V.; Eliav, E. *J. Phys. Chem. A.* **2009**, *113*, 12504. (b) Réal, F.; Vallet, V.; Marian, C.; Wahlgren, U. *J. Chem. Phys.* **2007**, *127*, 214302.
(34) Pierloot, K.; van Besien, E. *J. Chem. Phys.* **2005**, *123*, 204309.
(35) (a) Pierloot, K.; van Besien, E.; van Lenthe, E.; Baerends, E. J. *J. Chem. Phys.* **2007**, *126*, 194311. (b) van Besien, E.; Pierloot, K.; Görller-Walrand, C. *Phys. Chem. Chem. Phys.* **2006**, *8*, 4311.
(36) Matsika, S.; Pitzer, R. M. *J. Phys. Chem. A.* **2001**, *105*, 637.
(37) Grenthe, I.; Fuger, J.; Konings, R. J. M.; Lemire, R. J.; Muller, A. B.; Nguyen-Trung, C.; Wanner, H. *Chemical Thermodynamics of Uranium. NEA-TDB*; OECD, Nuclear Energy Agency Data Bank; Elsevier/North Holland: Amsterdam, The Netherlands, 1992.
(38) Neese, F. *Coord. Chem. Rev.* **2009**, *253*, 526.
(39) Wei, F.; Wu, G. S.; Schwarz, W. H. E.; Li, J. *Theor. Chem. Acc.*, **2011**, DOI: 10.1007/s00214-010-0885-5.
(40) Wei, F.; Wu, G.-S.; Li. J. *J. Chem. Theory Comput.*, in press.
(41) *ADF 2007.01*; SCM, Theoretical Chemistry, Vrije Universiteit: Amsterdam, The Netherlands (http://www.scm.com). (a) Fonseca Guerra, C.; Snijders, J. G.; te Velde, G.; Baerends, E. *J. Theor. Chem. Acc.* **1998**, *99*, 391. (b) te Velde, G.; Bickelhaupt, F. M.; van Gisbergen, S. J. A.; Fonseca Guerra, C.; Baerends, E. J.; Snijders, J. G.; Ziegler, T. *J. Comput. Chem.* **2001**, *22*, 931.
(42) Perdew, J. P.; Burke, K.; Ernzerhof, M. *Phys. Rev. Lett.* **1996**, *77*, 3865.
(43) van Lenthe, E.; Baerends, E. J. *J. Comput. Chem.* **2003**, *24*, 1142.
(44) (a) van Lenthe, E.; Ehlers, A. E.; Baerends, E. J. *J. Chem. Phys.* **1999**, *110*, 8943. (b) van Lenthe, E.; Baerends, E. J.; Snijders, J. G. *J. Chem. Phys.* **1994**, *101*, 9783. (c) van Lenthe, E.; Baerends, E. J.; Snijders, J. G. *J. Chem. Phys.* **1993**, *99*, 4597. (d) van Lenthe, E.; Snijders, J. G.; Baerends, E. J. *J. Chem. Phys.* **1996**, *105*, 6505. (e) van Lenthe, E.; van Leeuwen, R.; Baerends, E. J.; Snijders, J. G. *Int. J. Quantum Chem.* **1996**, *57*, 281.
(45) van Duijneveldt, F. B.; van Duijneveldt-van de Rijdt, J. G. C. M.; van Lenthe, J. H. *Chem. Rev.* **1994**, *94*, 1873.
(46) (a) Klamt, A.; Schüürmann, G. *J. Chem. Soc., Perkin Trans 2* **1993**, 799. (b) Pye, C. C.; Ziegler, T. *Theor. Chem. Acc.* **1999**, *101*, 396.
(47) Allinger, N. L.; Zhou, X.; Bergsma, J. *J. Mol. Struct. (THEOCHEM)* **1994**, *312*, 69.
(48) (a) Lee, B.; Richards, F. M. *J. Mol. Biol.* **1971**, *55*, 379. (b) Richards, F. M. *Annu. Rev. Biophys. Bioeng.* **1977**, *6*, 151.
(49) (a) Connolly, M. L. *J. Appl. Crystallogr.* **1983**, *16*, 548. (b) Connolly, M. L. *J. Mol. Graphics Modell.* **1993**, *11*, 139.
(50) The SES option was used in Figures 3 and 5 and in Table 3 with single-point COSMO calculations at optimized gas-phase geometries. The SAS option was used in Tables 1, 2, and 4 with geometry optimizations with COSMO.
(51) (a) Ben-Naim, A.; Marcus, Y. *J. Chem. Phys.* **1984**, *81*, 2016. (b) McQuarrie, D. A.; Simon, J. D. *Molecular Thermodynamcis*; University Science Books: Sausalito, CA, 1999.
(52) Wang, F.; Ziegler, T.; van Lenthe, E.; van Gisbergen, S.; Baerends, E. J. *J. Chem. Phys.* **2005**, *122*, 204103.
(53) Schipper, P. R. T.; Gritsenko, O. V.; van Gisbergen, S. J. A.; Baerends, E. J. *J. Chem. Phys.* **2000**, *112*, 1344.
(54) (a) Lee, S. Y.; Heller, E. J. *J. Chem. Phys.* **1979**, *71*, 4777. (b) Heller, E. J.; Sundberg, R. L.; Tannor, D. *J. Phys. Chem.* **1982**, *86*, 1822. (c) Heller, E. *J. Acc. Chem. Res.* **1981**, *14*, 368. (d) Tannor, D. J.; Heller, E. J. *J. Chem. Phys.* **1982**, *77*, 202.
(55) (a) Neese, F.; Petrenko, T.; Ganyushin, D.; Olbrich, G. *Coord. Chem. Rev.* **2007**, *251*, 288. (b) Petrenko, T.; Neese, F. *J. Chem. Phys.* **2007**, *127*, 164319.
(56) (a) Acosta, A.; Zink, J. I. *J. Organomet. Chem.* **1998**, *554*, 87. (b) Bailey, S. E.; Eikey, R. A.; Abu-Omar, M. M.; Zink, J. I. *Inorg. Chem.* **2002**, *41*, 1755.
(57) Fonger, W. H.; Struck, C. W. *J. Chem. Phys.* **1974**, *60*, 1994.
(58) (a) Wilson, E. B.; Decius, J. C.; Cross, P. C. *Molecular Vibrations: The Theory of Infrared and Raman Vibrational Spectra*; McGraw-Hill: New York, 1955. (b) McHale, J. L. *Molecular Spectroscopy*; Prentice Hall: Upper Saddle River, NJ, 1999.
(59) de Jong, W. A.; Visscher, L.; Nieuwpoort, W. C. *J. Mol. Struct. (Theochem)* **1999**, *458*, 41.
(60) Straka, M.; Dyall, K. G.; Pyykkö, P. *Theor. Chem. Acc.* **2001**, *106*, 393.
(61) Jackson, V. E.; Craciun, R.; Dixon, D. A.; Peterson, K. A.; de Jong, W. A. *J. Phys. Chem. A* **2008**, *112*, 4095.
(62) Hay, P. J.; Martin, R. L.; Schreckenbach, G. *J. Phys. Chem. A* **2000**, *104*, 6259.
(63) Siboulet, B.; Marsden, C. J.; Vitorge, P. *Chem. Phys.* **2006**, *326*, 289.
(64) (a) Vallet, V.; Moll, H.; Wahlgren, U.; Szabó, Z.; Grenthe, I. *Inorg. Chem.* **2003**, *42*, 1982. (b) Vázquez, J.; Bo, C.; Poblet, J. M.; de Pablo, J.; Bruno, J. *Inorg. Chem.* **2003**, *42*, 6136. (c) Ikeda, A.; Hennig, C.; Tsushima, S.; Takao, K.; Ikeda, Y.; Scheinost, A. C.; Bernhard, G. *Inorg. Chem.* **2007**, *46*, 4212. (d) Boulet, B.; Joubert, L.; Cote, G.; Bouvier-Capely, C.; Cossonnet, C.; Adamo, C. *Inorg. Chem.* **2008**, *47*, 7983. (e) Ikeda-Ohno, A.; Hennig, C.; Tsushima, S.; Scheinost, A. C.; Bernhard, G.; Yaita, T. *Inorg. Chem.* **2009**, *48*, 7201.
(65) Bismondo, A.; Casellato, U.; Sitran, S. *Inorg. Chim. Acta* **1985**, *110*, 205.
(66) Wada, G.; Tamura, E.; Okina, M.; Nakamura, M. *Bull. Chem. Soc. Jpn.* **1982**, *55*, 3064.
(67) Klamt, A. *Cosmo-RS: from quantum chemistry to fluid phase thermodynamics and drug design*; Elsevier: Amsterdam, The Netherlands, 2005.
(68) Sinnecker, S.; Rajendran, A.; Klamt, A.; Diedenhofen, M.; Neese, F. *J. Phys. Chem. A* **2006**, *110*, 2235–2245.
(69) *Lange's Handbook of Chemistry* , 15th ed.; Dean, J. A., Ed.; McGraw-Hill: New York, 1999.
(70) de Oliveira, C. A. F.; Hamelberg, D.; McCammon, J. A. *J. Phys. Chem. B* **2006**, *110*, 22695.
(71) Billard, I.; Geipel, G. *Springer Ser. Fluoresc.* **2008**, *5*, 465.
(72) (a) Bell, J. T.; Biggers, R. E. *J. Mol. Spectrosc.* **1965**, *18*, 247. (b) Bell, J. T.; Biggers, R. E. *J. Mol. Spectrosc.* **1968**, *25*, 312.
(73) Herzberg, G. *Molecular Spectra and Molecular Structure. I. Spectra of Diatomic Molecules*; Van Nostrand Reinhold Company: New York, 1950.
(74) Kasha, M. *Faraday Discuss.* **1950**, *9*, 14.